5-2016

A New Low-Cost Microstrip Antenna Array for 60 GHz Applications

Darwin J. Joaquin
Utah State University

A NEW LOW-COST MICROSTRIP ANTENNA ARRAY FOR 60 GHZ APPLICATIONS

by

Darwin J. Joaquin

A thesis submitted in partial fulfillment
of the requirements for the degree

of

MASTER OF SCIENCE

in

Electrical Engineering

Approved:

Dr. Bedri A. Cetiner Major Professor	Dr. Reyhan Baktur Committee Member
Dr. Jacob Gunther Committee Member	Dr. Mark R. McLellan Vice President for Research and Dean of the School of Graduate Studies

UTAH STATE UNIVERSITY
Logan, Utah

2016

Abstract

A New Low-Cost Microstrip Antenna Array for 60 GHz Applications

by

Darwin J. Joaquin, Master of Science

Utah State University, 2016

Major Professor: Dr. Bedri A. Cetiner
Department: Electrical and Computer Engineering

In this thesis, the design, fabrication, and characterization of a 2×8 microstrip planar antenna array operating at the 60 GHz band for Wireless Gigabit Alliance (WiGig) applications are presented. The trade-offs among low production costs, performance, and ease of fabrication were considered. Full-wave electromagnetic (EM) analysis is implemented for the antenna design by using ANSYS®High Frequency Structural Simulator (HFSS), a finite-element EM solver. The antenna structure consists of two layers, where each array element is a Conductor-Backed Coplanar Waveguide (CB-CPW) loop-fed patch antenna. The bottom layer houses the transmission line and feeding circuitry, while the patch antennas are built on the top layer. The transmission line is designed on microfabrication-compatible quartz substrate, and the patches on a Rogers RO3003 Printed Circuit Board (PCB) substrate. The CPW network's right-angle bends are optimized with chamfered lines. Air bridges are used to suppress the parasitic coupled slot line mode of the CPW line divisions. Results of the EM analysis show that the array covers the United States (US) 60 GHz unlicensed band (57-64 GHz), and has a maximum realized gain of 18 dB at 61 GHz on the broadside direction. The antenna design is later fabricated combining microfabrication and standard PCB procedures.

(45 pages)

Public Abstract

A New Low-Cost Microstrip Antenna Array for 60 GHz Applications

by

Darwin J. Joaquin, Master of Science

Utah State University, 2016

Major Professor: Dr. Bedri A. Cetiner
Department: Electrical and Computer Engineering

The use of telecommunications and the amount of data exchanged continue to grow at exponential rates. New technologies allowing for higher data transfer speeds while keeping the products affordable are required. Among these technologies, the WiGig protocol promises to be a shorter-range complement for high-speed Wi-Fi. One of the most important elements in a communication system are the antennas. For this reason, it is of great interest to have antennas that keep on pace with the other elements of the system. It is important to have affordable and high performance antennas to expand the use of the technology. This research deals with the design, fabrication, and characterization of one such antenna. The trade-offs between low production cost, ease of fabrication, and performance are considered. This thesis describes the techniques used for improving the performance of the antenna feeding. The combined use of inexpensive microfabrication and standard Printed Circuit Board (PCB) fabrication procedures allow the antenna to maintain low costs without considerable compromise in performance.

To my beloved family...

Acknowledgments

I would like to thank my advisor Dr. Bedri Cetiner. He is the one that gave me the opportunity to work on this research as a part of his group. He gave me the tools and support necessary to advance my work and to learn how to be a good researcher and professional. Dr. Cetiner and the colleagues in Turkey also took responsibility of the microfabrication process. All information and pictures regarding said process have come from them.

I would also like to thank all my friends here in Logan. They have been like a family to me. I appreciate all the support and the unforgettable moments. They made my stay here a highlight of my life. I want to thank my beloved family, who would always show their care and support from afar. Even if they didn't like me being away for so long, they would always understand and help in any way they could. Without them I wouldn't even think of being here.

I am very grateful to the government of the Dominican Republic, who by way of their Ministry of Higher Education covered most of my expenses while was here. I am also thankful to everybody in the International Programs division of the USU Office of Global Engagement for their constant personal, economic, and general social support. They have made this experience possible.

Darwin J. Joaquin Pimentel

Contents

List of Tables

List of Figures

Acronyms

HFSS	High Frequency Structure Simulator
CPW	Coplanar Waveguide
CB	Conductor-Backed
PCB	Printed Circuit Board
RF	Radio Frequency
WiGig	Wireless Gigabit Alliance
PEC	Perfect Electric Conductor
3-D	Three-dimensional
BW	Bandwidth
EM	Electromagnetic
VNA	Vector Network Analyzer

Chapter 1

Introduction

Telecommunications have experienced an exponential growth over the past three decades. The amount of data the average person uses keeps increasing at exponential rates in the present day [1]. This growth is more noticeable when looking at the evolution of wireless communications [2]. The needs for higher speed have increased accordingly, making researchers search for means to improve the data rates.

The portion of the electromagnetic (EM) spectrum that is currently used for mass wireless communications (cellular, Wi-Fi, Bluetooth, etc.) sits around the 0.5-6 GHz region, which is a fraction of the spectrum, and considerably crowded. This is a limiting factor even when considering the great advances made in spectral efficiency [3]. Engineers and scientists have been working for a long time studying other portions of the spectrum that can be used to develop wireless technologies [4]. The unlicensed 60 GHz band is one of these portions. Previously used only for point-to-point radio links (e.g. satellite-to-satellite communications), this band currently houses several short-range high-throughput wireless technologies. Among these are WirelessHD and Wireless Gigabit Alliance (WiGig, the trade association that developed the technology).

WiGig allows devices to communicate at multi-gigabit-per-second speeds [5]. It has received a considerable commercial boost thanks to the acquisition of related start-up companies by technology giants. Other smaller ventures keep appearing, which allow for a diversification of the offered compliant devices. Several WiGig chipsets are already sold online [6–8]. As a parallel to this, research on the WiGig systems has become widespread in the past couple of years [9–12]. A greater expansion can be achieved with antennas designed with a balance of price and performance. Among the components of a wireless communications systems, the antenna plays an essential part for the performance and integration.

At 60 GHz, the rain attenuation is high, and the electromagnetic losses are significant. More importantly, at this exact frequency there is a peak in oxygen absorption [13]. Figure 1.1 shows the atmospheric attenuation at millimeter-wave frequencies. Hence the use of WiGig for indoor coverage.

There is as much as 9 GHz of bandwidth in this unlicensed band, depending on the country. In North America the 60 GHz band covers from 57 to 64 GHz [5]. An antenna compatible with these applications needs to have a large bandwidth that covers the entire WiGig band. The short-range applications work as point-to-point radio links, and as such need a high directivity and gain.

The objective of this research is to design a new model of antenna for use in WiGig communications. This antenna should be able to compete with comparable antennas in performance, while also keeping a lower-cost manufacturing process. Antennas for 60 GHz have been designed and fabricated years before the standardization of WiGig [15–17]. With the recent peak in research, antennas have started being designed using a wide variety of materials, feeding networks, and fabrication techniques [18–21], trying to get the balance of performance and cost. A maximum gain of 18 dB, and a bandwidth that covers the entire US WiGig band are targeted. The designed product is a Microstrip (patch) antenna, with a total thickness under 1 mm. The accessibility of the materials and ease of manufacturing are taken into account, as well as the effect of these on the performance. The research follows on the steps of previous works on 60 GHz antennas made by members of the research team [22].

This thesis documents the steps followed to obtain a 60 GHz antenna with the desired features. For the whole design process, full-wave EM analysis is done by using ANSYS's High Frequency Structural Simulator (HFSS) [23], a finite-element EM solver. Keysight's Advanced Design System (ADS) [24] is also used in the design and calculation of the transmission lines. Initially, a single antenna is designed. Although its figures of merit do not comply with the expected values for gain and bandwidth, it serves as a main building block for a larger antenna array. The design process of the single-element antenna is detailed in Chapter 2. Later, the larger array is designed based on the single antenna. This a planar

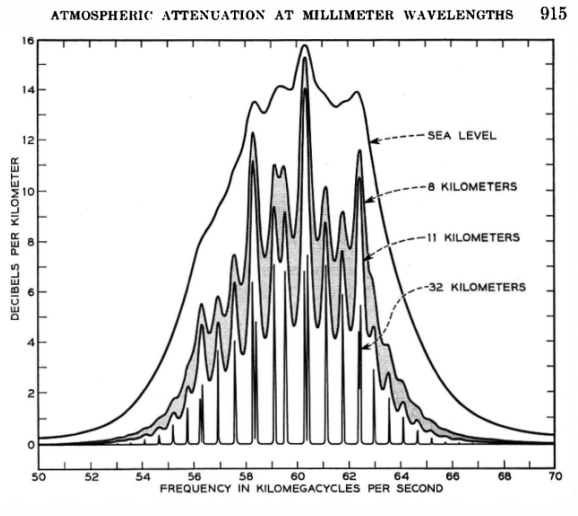

Fig. 1.1: Atmospheric attenuation at millimeter-waves. Source: Crawford and Hogg [14]

array with 2×8 elements. The complex feeding network and the design challenges are explained in Chapter 3. The fabrication process is included on Chapter 4. The conclusion and commentary on the next research steps are done in the last chapter.

Chapter 2

Single-element Wireless Gigabit Alliance Antenna

2.1 Transmission Line and Material Selection

The accurate design and full-wave EM analysis of a single-element antenna is the primordial step on the design of the antenna array. A single microstrip patch antenna cannot achieve the goal for total gain that is required for WiGig applications. However, it is the basic building block of the antenna array. After comparing the performance of the antenna with different feeding mechanisms (such as microstrip line, inset coaxial line, aperture coupling, and coplanar waveguide) the decision was made to use a Conductor-Backed Coplanar Waveguide (CB-CPW) loop-feed. Among the reasons for the choice are: the ease of fabrication, the lower radiation loss, and the fact that the characteristic impedance can be determined by a ratio [25]. This last item facilitates size modification at higher frequencies. The CB-CPW is a variation of the conventional CPW with a lower ground plane [26]. The lower ground provides mechanical strength for thin and fragile substrates. More importantly for the present project, it serves to achieve a directional radiation pattern. This antenna structure consists of two substrate layers: one lower layer that includes the $50-\Omega$ CPW-fed loop, and an upper layer that contains the radiating coupled patch antenna (see Figure 2.1). The CPW line consists of the main conductor strip (S), and the two adjacent slots (W) that separate the center conductor from the coplanar grounds. A design specification that needs to be followed is to keep the width of S at 0.191 mm. This assures that the fabricated antenna is compatible in size with the available micro-probes. The probe station interfaces to a Vector Network Analyzer (VNA), which is used to measure the reflection coefficient and radiation patterns of the antenna. The loop in the lower layer is a rectangular slot which enables EM energy to couple to the patch on the top layer. The patch is a rectangular-shaped metal built on top of the upper substrate.

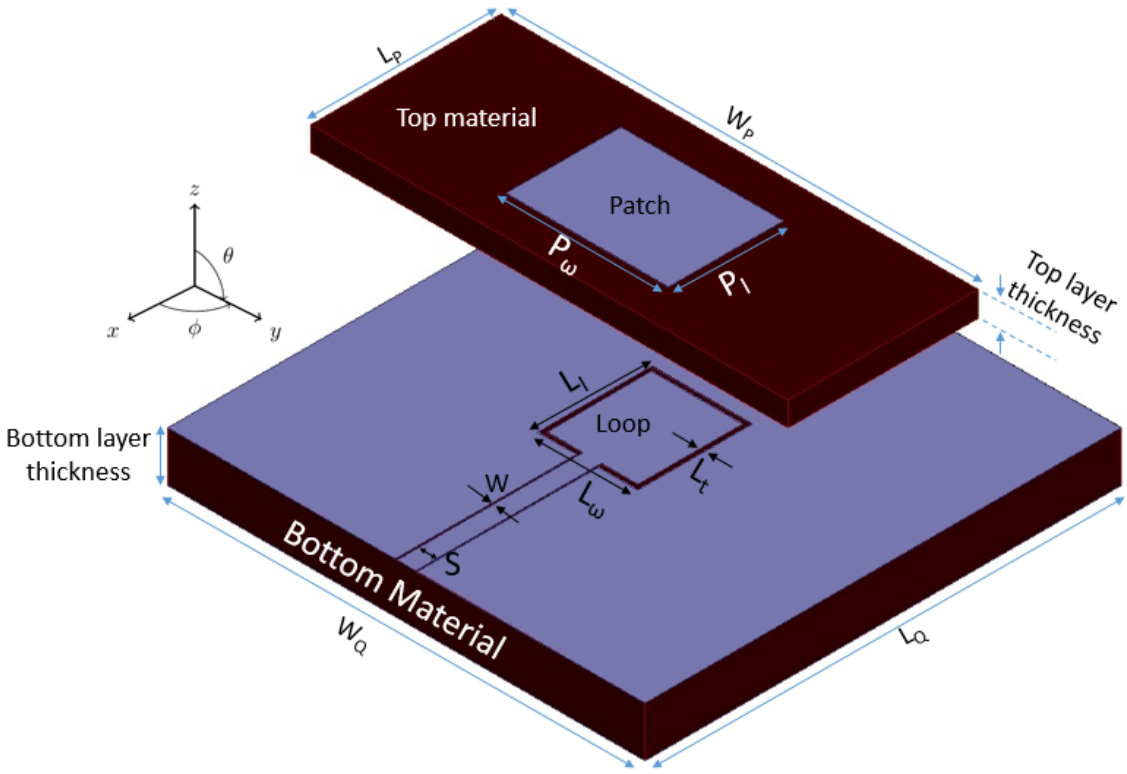

Fig. 2.1: 3-D view of the single-element antenna with upper wafer separated for the sake of illustration

Initially, the design was made using microfabrication compatible quartz substrate ($\epsilon_r = 3.9, \tan\delta = 0.0002$) for both layers. This material has been previously used for 60 GHz antenna design by members of the same research team [22, 27]. The lower layer was designed on a 525-µm-thick substrate and the upper layer on a 200-µm-thick substrate. These substrates are coated by a 2-µm-thick copper layer by a thin film metal deposition process. The decision was made later to change the design material of both layers to printed circuit board (PCB) material. That would lower the antenna costs for materials and fabrication. The feed network type remained the same. The 50−Ω CPW transmission line, loop, and patch dimensions would be calculated for the new material. Several options were explored for the material selection. The Rogers®RO3003 substrate was selected because of its favorable properties for millimeter-wave fabrication, its affordable price, and because it possesses the lowest losses among Rogers's commercial line level laminates. The RO3003 also comes with an option for rolled copper as the cladding, which according to the manufacturer helps decrease the insertion losses. For the PCB design, there is a lower amount of thicknesses that can be accomplished because of these being fixed in a purchased laminate. With the goal of having similar dimensions to the all-quartz antenna, the thicknesses selected were 0.508 mm for the bottom layer and 0.254 mm for the top layer. Table 2.1 shows a summary of the properties of the PCB materials that were considered for the project.

2.2 Antenna Design

The dimensions of the loop are based on the half-wavelength resonance Equation

$$L_l + L_\omega/2 \sim \lambda_g/2 \tag{2.1}$$

Table 2.1: Comparisons of Rogers substrates

Material	Dielectric Constant	Dissipation Factor	Relative Price
Rogers RO3003	3.00	0.0010	2
Rogers RO3203	3.02	0.0016	2.1
Rogers RO4003C	3.38	0.0027	1
Rogers RT/duroid 5880	2.20	0.0009	6

where L_l and L_ω are the length and width of the loop, respectively (see Figure 2.1). λ_g is the guide wavelength on quartz at the design frequency. The patch metalization is centered over the loop, and its calculated dimensions are given by the following equations [28]:

$$P_l \sim \frac{c}{2 * f_p * \sqrt{\epsilon_r}} \tag{2.2}$$

$$P_l < P_\omega < 2P_l \tag{2.3}$$

where P_l and P_ω represent the patch length and width (see Figure 2.1), c is the speed of light in vacuum, f_p is the patch design frequency, and ϵ_r is the relative permittivity of the material. The loop and patch antenna dimensions are optimized so that they share the same resonance frequency. It should be noted that the upper substrate length is shorter than the lower one ($L_p < L_Q$). The main advantage for that design decision is the added room to access the feeding line for measurement purposes.

Early simulation results for the single antenna showed a realized gain of 7 dB on the broadside direction (see Figures 2.2(a) and 2.2(b)). The impedance bandwidth shows to be narrower than expected (Figure 2.3). After the finalization of the design process for the PCB antenna, a fabrication limitation arose: the commercial PCB manufacturers are not capable of producing the feed network with the specified dimensions (CPW 50−Ω transmission line slot with 20 µm width) by standard procedures. Although fabrication is possible, the cost is prohibitive to try this solution. To overcome this issue, it was decided to change the lower substrate from PCB to quartz. Doing so would allow the use of the microfabrication techniques already mentioned before to fabricate the feed network of the antenna while keeping the price low. The RO3003 was kept as the upper substrate, which maintains the uniqueness of the design and allows that the radiating layer remains easy and accessible to fabricate. The parameters and dimensions for both the CPW loop-feed and the patch antenna were modified for an optimal impedance bandwidth and radiation pattern. The final dimensions are shown in Table 2.2. A simple schematic of the antenna layers is shown on Figure 2.4.

Table 2.2: Design parameters of the single-element quartz + PCB WiGig antenna (all dimensions are in mm)

Parameter	Value	Parameter	Value
S	0.191	W	0.02
L_l	1.2	L_ω	1.05
L_t	0.05	P_l	1.20
P_ω	1.7	L_P	2
W_Q	7	L_Q	7

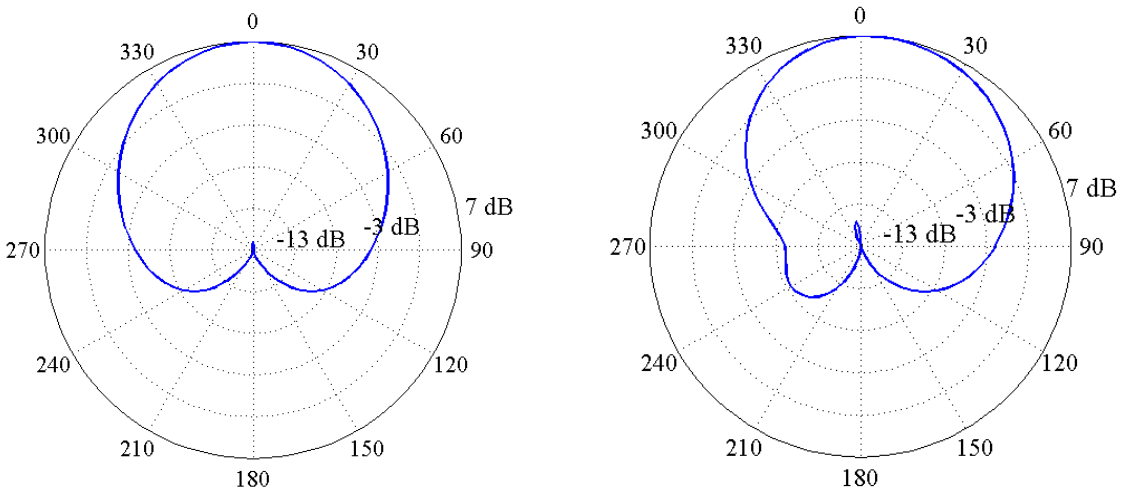

(a) Realized gain pattern in the yz plane

(b) Realized gain pattern in the xz plane

Fig. 2.2: Simulated radiation pattern plots showing the realized gain of the PCB antenna at 60 GHz

The maximum realized gain of the quartz + PCB single antenna on the broadside direction is 7.2 dB at 60 GHz. An increase in the gain can be attributed to the fact that quartz has less material loss than the PCB substrate previously used for the bottom layer. Figure 2.5 shows the 2-D radiation pattern of the single antenna on the YZ and XZ planes. The simulated radiation patterns also show the antenna to be linearly polarized (see Figure 2.6). Figure 2.7 shows the reflection coefficient of the single antenna. It presents an impedance bandwidth of close to 6 GHz around the main 60 GHz frequency. The realized gain across the frequency range of interest for the single antenna in the broadside direction is presented in the same figure. The gain remains over 5 dB for the whole frequency range.

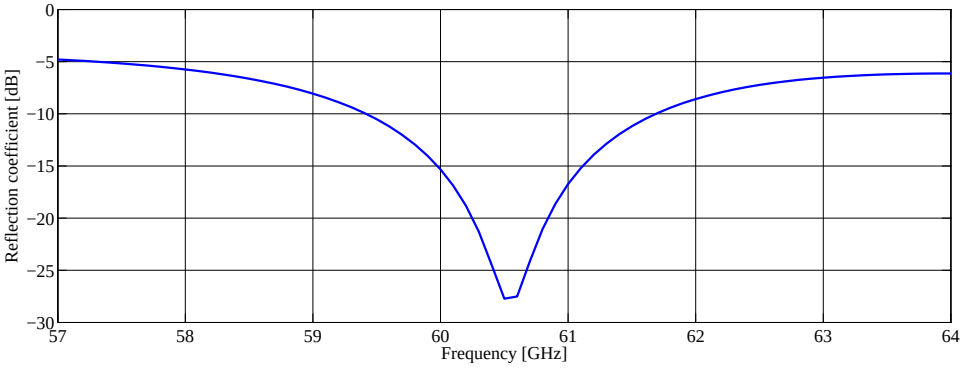

Fig. 2.3: Simulated reflection coefficient of the PCB single antenna

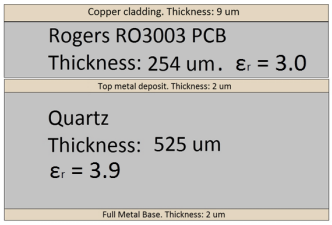

Fig. 2.4: Schematic depicting the materials of the 60 GHz antenna

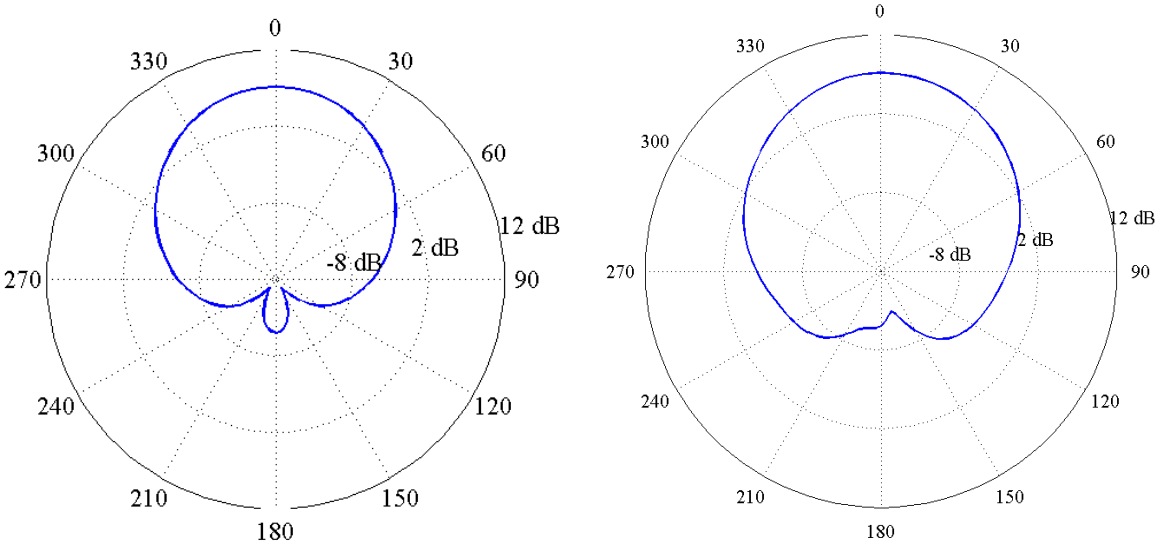

(a) Realized gain pattern in the yz plane

(b) Realized gain pattern in the xz plane

Fig. 2.5: Radiation pattern plots showing the realized gain of the antenna at 60.7 GHz

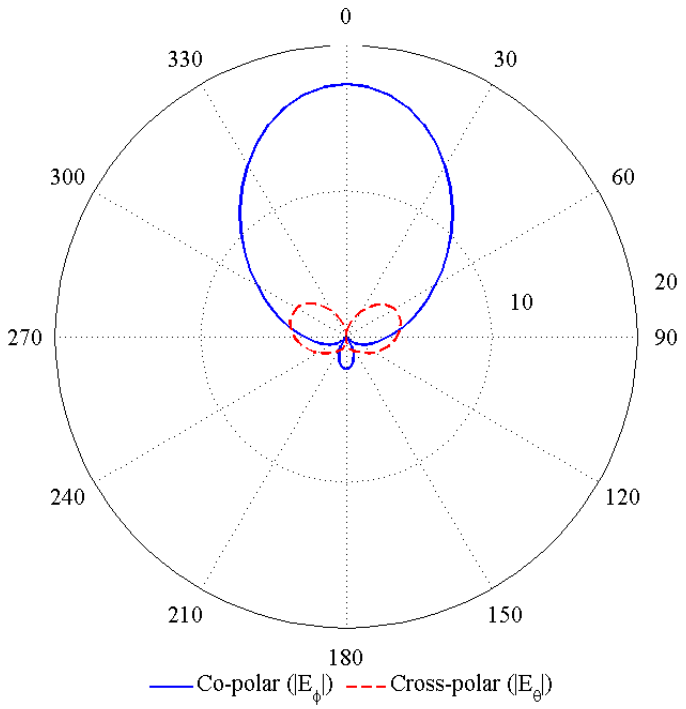

Fig. 2.6: Simulated magnitudes of electric field components on broadside direction at 60 GHz

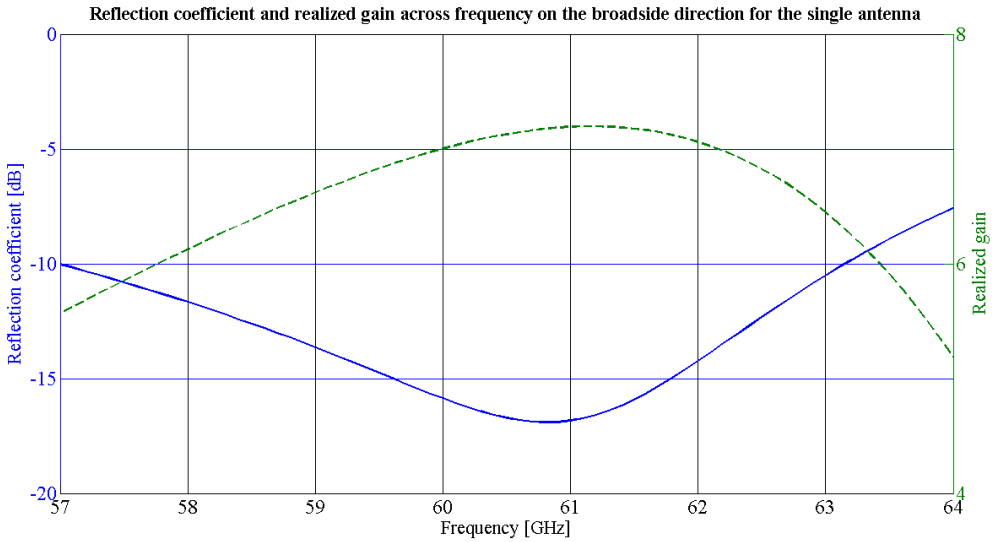

Fig. 2.7: Reflection coefficient and realized gain across frequency on the broadside direction of the Single Antenna

Chapter 3

WiGig Antenna Array

The goal of the project is to design, fabricate, and characterize an antenna array with a realized gain around 18 dB and an impedance bandwidth (reflection coefficient < -10 dB) that covers the 57-64 GHz WiGig band. The final product is a 2×8 planar array based on the single-element antenna described in the previous chapter.

3.1 4-Element Antenna Array

For explaining the different elements that comprise and improve the feeding network, it is better to picture the 16-element array as a linear combination of four 2×2 antenna arrays. As such, the element separation remains identical when increasing the amount of elements from 4 to 16. The modeling of the 4-element array helps explain the 16-element array in a less convoluted way. A 3-D view of the 4-element antenna array is shown in Figure 3.1(a)

The array uses a corporate CPW feed network [29], with each single element being a CPW loop-feed patch antenna as previously described. The 50$-\Omega$ CPW feed line (S = 0.191 mm, and W = 0.02 mm as previously indicated) is divided into two 100$-\Omega$ lines (S = 0.0145 mm, W = 0.02 mm) by using a CPW T-junction power divider. The junction is formed by connecting the three center strip conductors on a T shape (see Figure 3.1(b)). The change in impedance is accomplished by changing the center strip's width while keeping the side slots width constant. As noted in the dimensions the value of W remains 0.02 mm while the value of S is changed from 0.191 to 0.0145 mm.

The 100-ohm impedance lines are transformed back to 50-ohm with quarter-wavelength transformers (see Figure 3.1(c)). The transformer impedance is given by

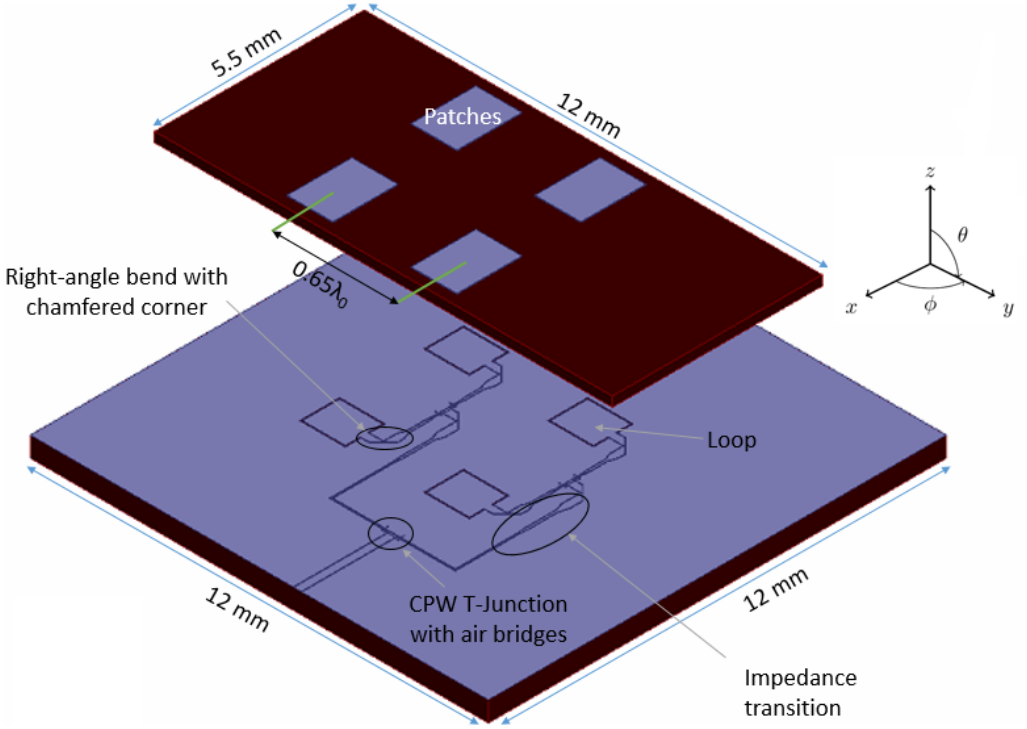

(a) 3-D view of the 4-element antenna array

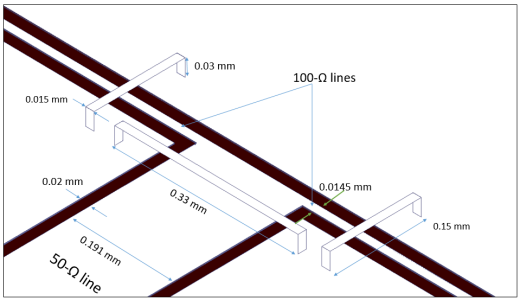

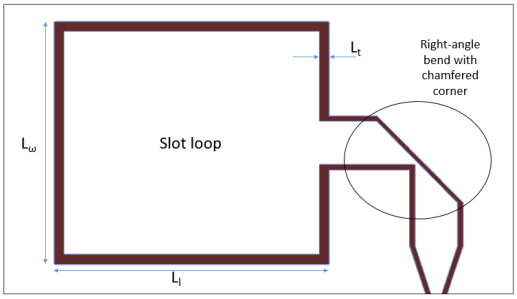

(b) CPW T-junction with air bridges, plus a close look of the right-angle bend an slot loop

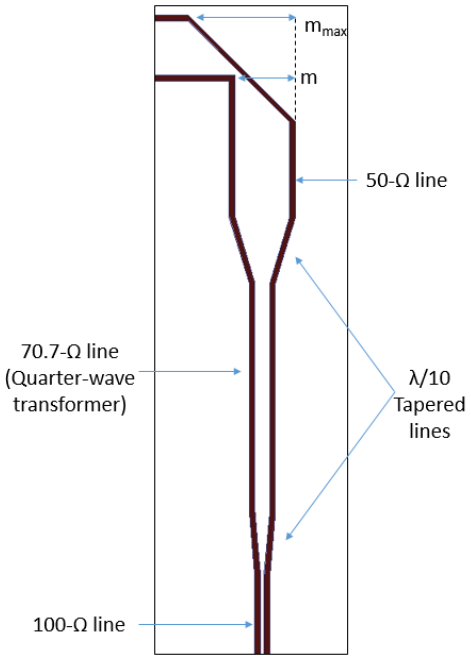

(c) Impedance transition and chamfered right-angle bend

Fig. 3.1: Schematic of the 2×2 antenna array. A close look at (b) the T-junction divider, slot loop, and (c) impedance transition are shown

$$Z_T = \sqrt{Z_0 Z_L} \tag{3.1}$$

where Z_T is the transformer's characteristic impedance, Z_0 is the input impedance (100 ohm), and Z_L is the load impedance (50 Ω). This results in a transformer section with a characteristic impedance of 70.7 Ω. In addition to the transformer, short tapered lines are used to make a smoother transition between the different impedances (seen in Figure 3.1(c)). Although the use of the tapering improves the transition performance, increasing its length has a negative effect on the impedance resonance. Each of these tapered lines was designed with a length shorter than $\lambda/10$, where λ is the effective wavelength in the fabrication material. The length was optimized to get an overall better impedance matching of the transmission line. Each branch of the transmission line goes through three right-angle bends on its path to the slot-loop (as shown in Figure 3.1(a)). Figure 3.1(b) also shows a close look at the slot loop with the immediate right-angle bend. A total of 8 bends are found in the 2×2 array. This number increases to 38 for the 2×8 antenna array. The reactance of these bends can cause performance degradation. Chamfering the corners is a simple and commonly used method that compensates for the bend reactance [30]. In Figure 3.1(c) the chamfer in the side ground plane is defined by the ratio of the distances m/m_{max}, and takes a value between 0 and 1.

For a given S/W (where S is the CPW signal strip width and W is the slot width, as explained in the previous chapter), the optimum chamfer for minimum return loss is given by

$$(\frac{m}{m_{max}}) = \begin{cases} 0.2102 \ln(\frac{S}{W}) + 0.7677 & \text{for } 0 \leqslant S/W \leqslant 2, \\ 1 & \text{for } S/W > 2.5. \end{cases} \tag{3.2}$$

For this antenna's transmission line the signal strip is much wider than the slots and therefore the latter case is used. After this the chamfering values have been optimized for a better impedance matching of the whole structure. The chamfers are applied to the 50-Ω bends, but not to the 100-Ω bends. The reason behind this is that through simulations of

the effects of the latter it was determined that the negligible difference in performance did not validate the added fabrication complexity.

The optimal mutual coupling between individual antenna elements was obtained when the element separation was 0.65-λ_0. Here λ_0 is the wavelength in the air at the design frequency of 60 GHz. At this separation, the best impedance and radiation performances are obtained. When using a CPW T-junction, discontinuities arise on the side ground planes. Moreover, an unwanted coupled slot-line mode is present in these cases. Air-bridges are used to suppress the parasitic coupled slot line mode, enforcing the single CPW mode operation of the microwave circuit. More importantly, the air bridges maintain continuity between the separated ground planes of the circuit. In the simulation environment, the air bridges are modeled as PEC structures of infinitesimal thickness (previously shown on Figure 3.1(b)), and a height between 3 and 30 µm. The width is chosen as 20 % over S+2*W, and slightly optimized for gain and bandwidth.

In theory, a four-element antenna array has a 6-dB gain over the base gain of the single-element antenna. Taking that into account, our 2 × 2 array has a theoretical gain of 13.2 dB (7.2 + 6 dB). The transmission line of the array introduces more losses into the overall radiation, and the 2 × 2 array's actual maximum realized gain is 12.3 dB (for transmission line losses of 0.9 dB, and an overall increase of 5.1 dB over the single element). Figure 3.2 shows the realized gain across the desired frequency band on the broadside direction.

The effect on performance of adding air bridges to the T-junctions of the 4-element

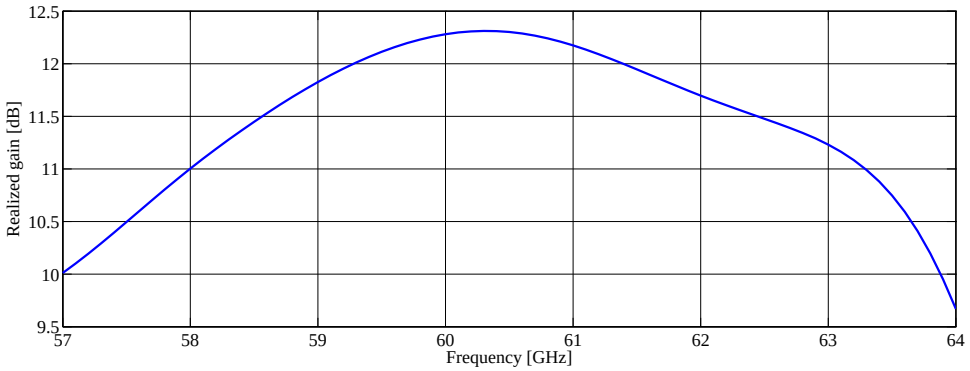

Fig. 3.2: Realized gain across frequency for the 4-element antenna

array is presented in Figures 3.3 and 3.4. The effect can be noted in both the impedance bandwidth and the realized gain. For the 4-element array, a 1.5 dB decrease in gain (from 12.3 to 10.8 dB) is observed if removing the air bridges. Although the total bandwidth does not decrease, the resonance with bridges has much better matching.

Air bridges can be found in literature used on the CPW right-angle bends with chamfered corners to suppress the parasitic slot line mode (see Figure 3.5). The effect of adding such air bridges was studied on the antenna array model. Figures 3.6 and 3.7 show the effects on impedance bandwidth and radiation pattern, respectively. The comparisons show that the addition of the extra bridges reduces the bandwidth of the antenna. The realized gain is also negatively affected, going from 12.3 dB with no extra bridges to 11.7 dB when adding them to the chamfered corners (an additional loss of 0.6 dB). Considering those effects it was decided to not add the extra bridges for the bends. The addition of those increases the complexity of the fabrication process while not showing performance improvement.

3.2 16-Element Antenna Array

The 16-element array is a linear combination of four of the presented 2×2 arrays. These 4-element arrays are combined with each other by using a CPW transmission line and the same power division techniques mentioned before. Figure 3.8 shows the full 16-element 3-D

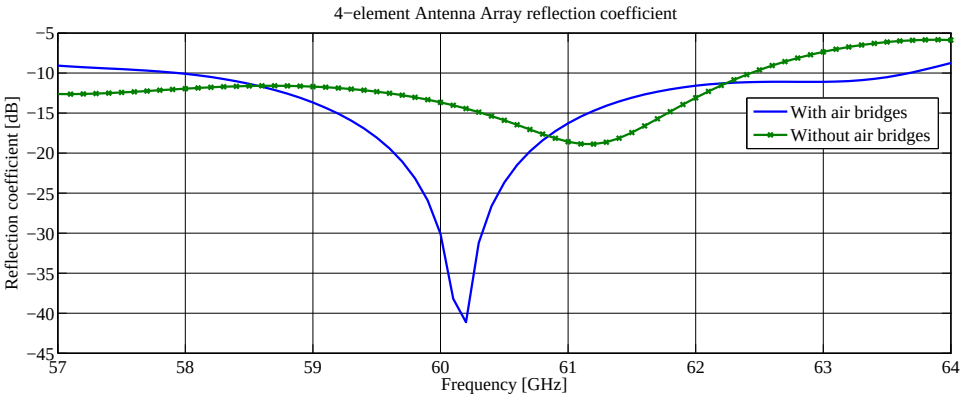

Fig. 3.3: Effect of air bridges on T-junctions of the 4-element antenna array reflection coefficient

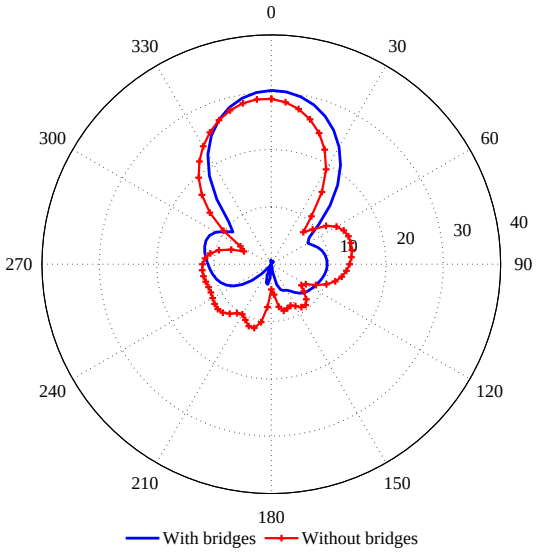

Fig. 3.4: Effect of air bridges on T-junctions of the 4-element antenna array radiation pattern at 60 GHz

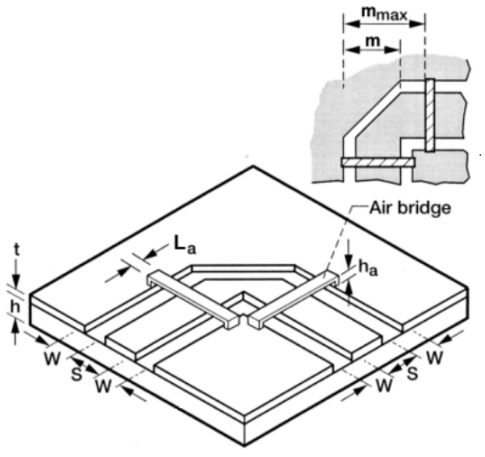

Fig. 3.5: Coplanar waveguide right-angle bend with chamfered corners and air bridges. Source: Simons [30]

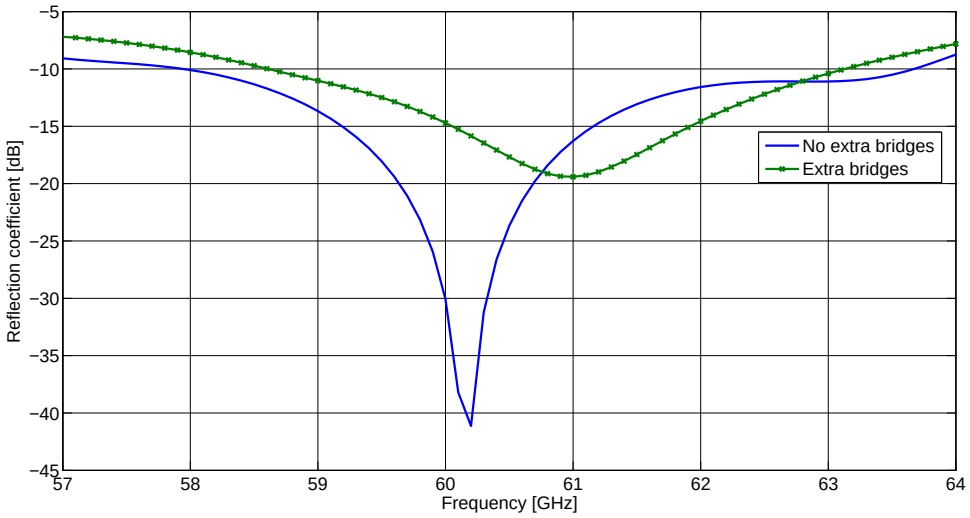

Fig. 3.6: Effect on impedance bandwidth of adding air bridges to the chamfered corners of the array

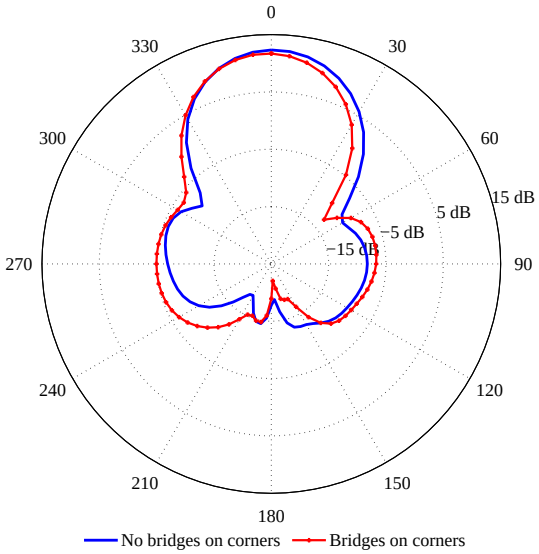

Fig. 3.7: Effect on the radiation pattern at 60 GHz on the broadside direction of adding air bridges to the chamfered corners of the array

model.

The finished simulated model has a maximum realized gain of 18.1 decibel on the broadside, with gain above 15 decibel across the entire desired band (see Figure 3.11). Figure 3.9 shows the 3-D radiation pattern of the antenna on the simulated environment. The model also shows an impedance bandwidth (reflection coefficient below -10 dB) that covers the entire WiGig frequency band. The reflection coefficient in the desired band is shown on Figure 3.10. The theoretical gain for the array is 19.2 dB. This value is obtained from the sum of the gain of the single antenna plus the array gain ($G_{SingleAntenna} + 10 \log 16$ = 7.2 + 16 = 19.2 dB). Based on the calculated gain, it is determined that the transmission line losses are 1.1 dB.

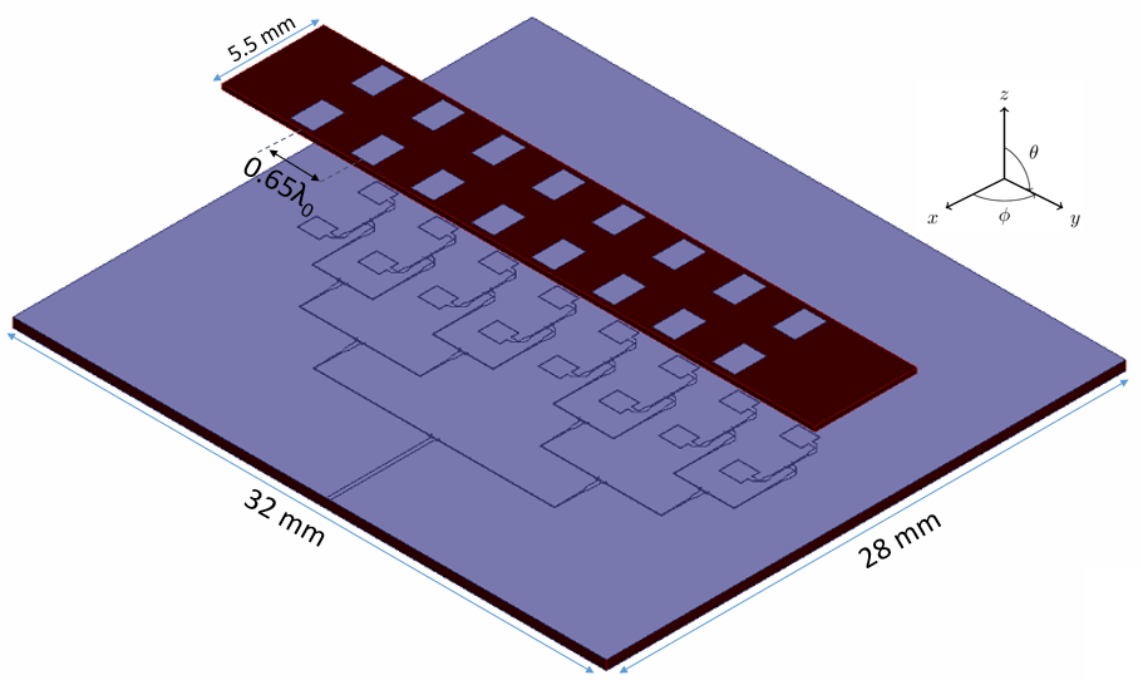

Fig. 3.8: 3-D View of the 2×8 Antenna Array Model

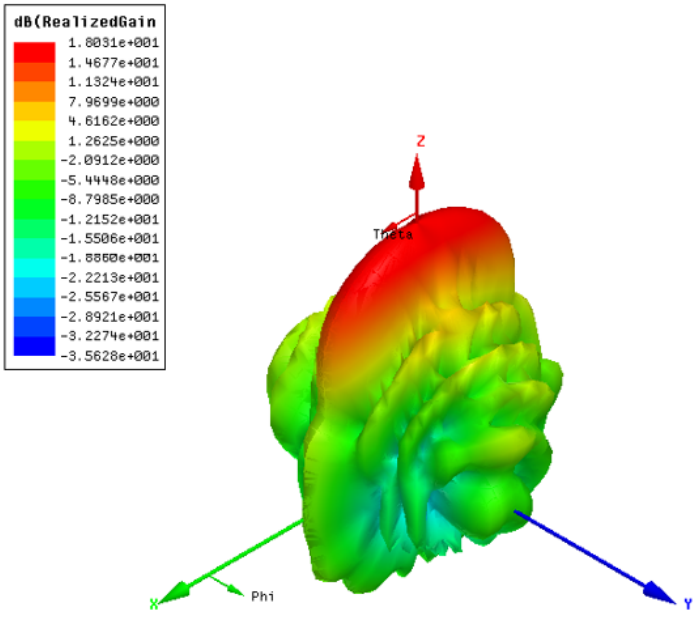

Fig. 3.9: 3-D Radiation pattern of the simulated 16-element antenna array at 61 GHz

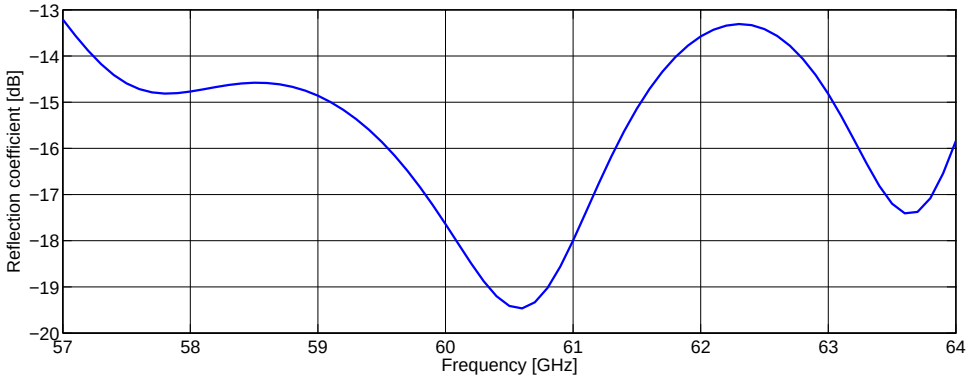

Fig. 3.10: Reflection coefficient of the simulated 16-element antenna array

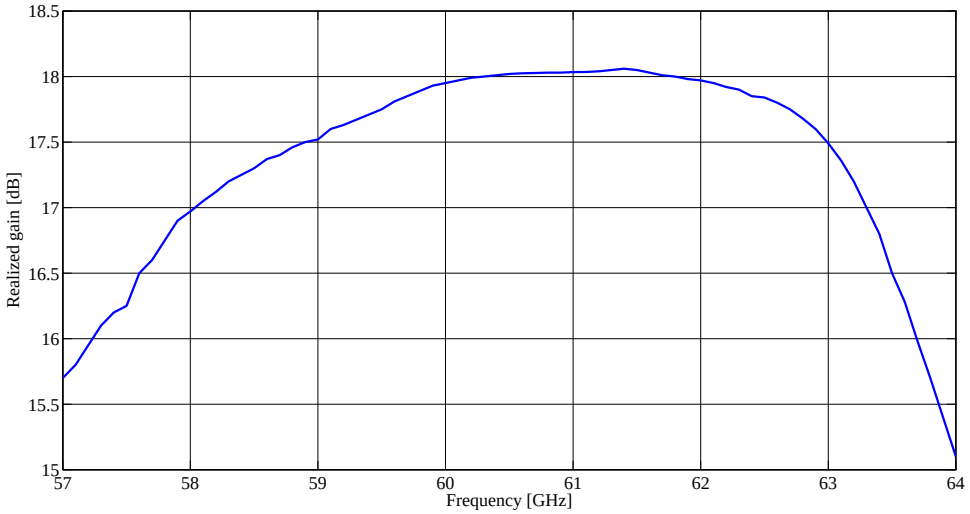

Fig. 3.11: Simulated realized gain across frequency for the 16-element array

Chapter 4

Fabrication

The fabrication process includes several stages. Due to the use of different materials for the antenna, each of these requires a specific fabrication procedure. The lower layer, which is built on RF-compatible quartz substrate, is built by a series of microfabrication processes. These processes are done at the Institute of Materials Science and Nanotechnology in Bilkent University, Turkey [31] (where USU has an ongoing joint Research and Development project). The process starts with a blank quartz wafer (represented in Figure 4.1). Then, the CPW transmission line and loops are fabricated, as well as a pair of bonding alignment marks. This is accomplished by depositing a thin (2 µm thick) copper layer via electron-beam deposition technique. The patterns of the CPW transmission line and loop are formed by a lift-off process on the metal. This is accomplished by adding a layer of copper by thin film deposition, while covering the desired slot areas of the design (Figure 4.2). The bonding alignments marks will be later used to align the lower and upper layers into one prototype.

Another layer of copper is added to the bottom of the quartz wafer by using the electron-beam technique. This represents the conductor-backing ground (see Figure 4.3, where the dark film on the bottom indicates the new ground layer). Afterwards, the quartz wafer is diced into pieces with the dimensions needed.

The microstrip antenna top layer includes the patch metalization. This layer is fabricated on a Rogers RO3003 PCB wafer ($\epsilon_r = 3.0, \tan\delta = 0.001$) by standard PCB fabrication techniques. A pair of bonding alignment marks identical to the ones on the lower layer are also added (see Figure 4.4). The PCB is then cut into the desired dimensions. The separate substrate layers are later bonded. The alignment marks are used to carefully place both in the correct position. A 3-D simulated view of the resulting single antenna is shown (Figure

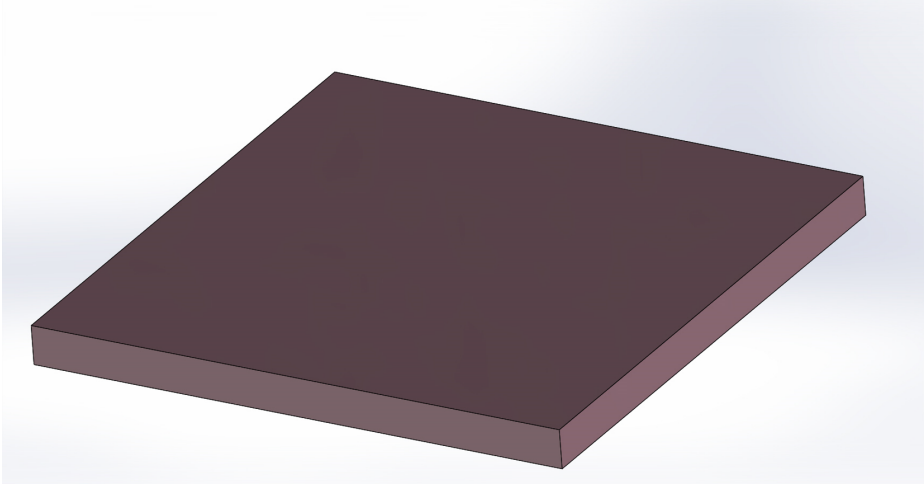

Fig. 4.1: Representation of the blank quartz wafer to be used in the microfabrication

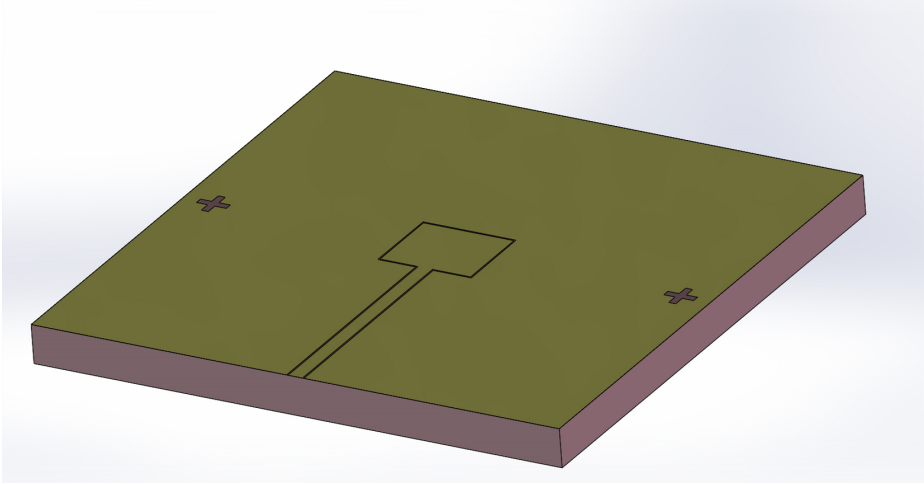

Fig. 4.2: A model of the microfabricated quartz wafer with CPW, loop and bonding alignments

4.5).

For the antenna array, the larger feeding network is fabricated following the same procedures from the single antenna. The fabrication of the array does add one more step to the process: the air bridges, which are not present in the single antenna. For practical purposes an air bridge can be substituted by wire bonds between the ground planes. The ends of the wire are bonded to the location where the air bridges make contact with the ground planes (refer back to Figure 3.1(b)). Putting a line of gold (or a similar metal) wire between the coplanar grounds where necessary, the sides are connected. The wire bonding

is done before the substrate bonding, which remains the last step. A simulated view of the final array is shown on Figure 4.6.

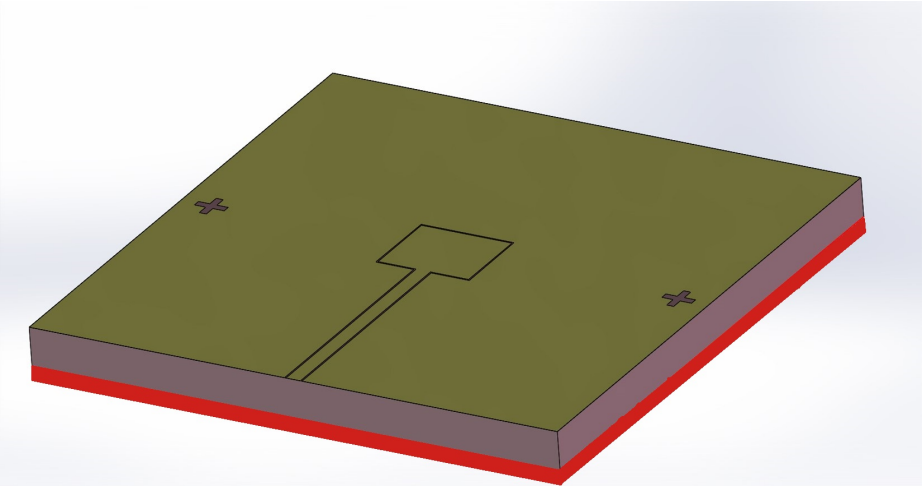

Fig. 4.3: Addition of the conductor-backing ground to the quartz wafer. It is represented here as a red layer on the bottom

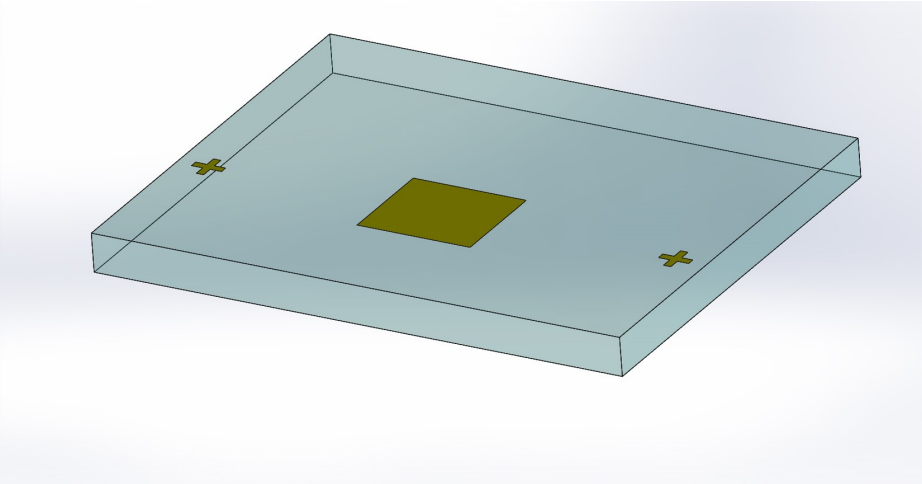

Fig. 4.4: Schematic of the PCB substrate with the patch and bonding alignment marks

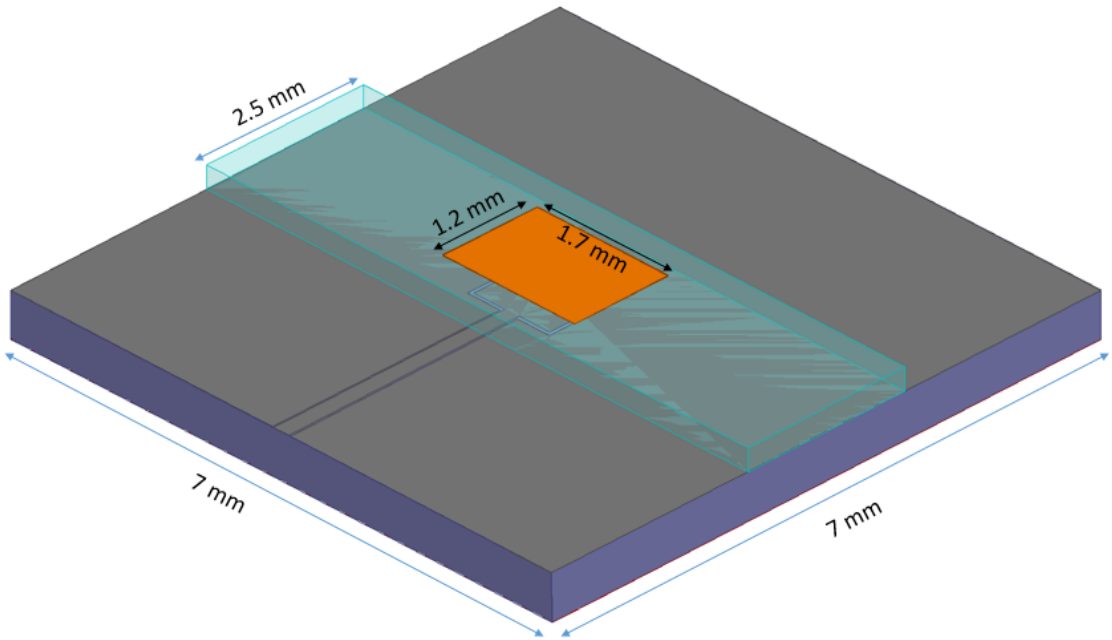

Fig. 4.5: Simulated 3-D view of a fabricated single-element antenna. The bonding alignments are not shown

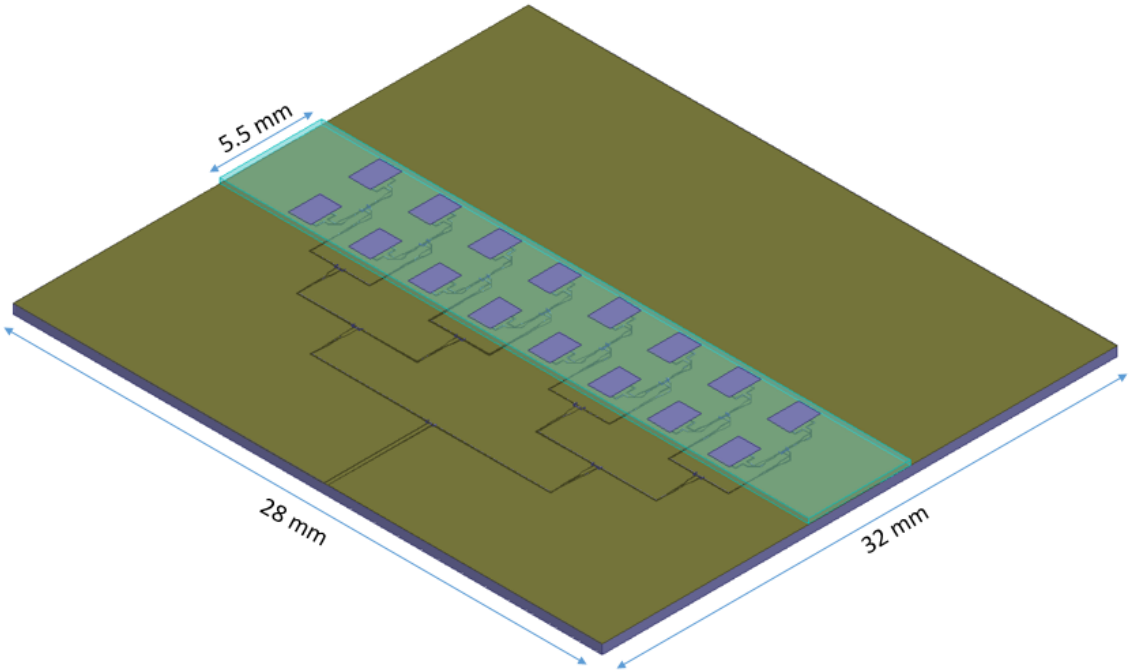

Fig. 4.6: A simulated view of the final 2×8 antenna array

Chapter 5

Conclusion and Future Work

The antenna array that combines micro-fabricated quartz and PCB substrate proves to be a viable low-cost addition to the WiGig antenna market. With less than 1 mm of total thickness and a maximum gain of 18 dB, as well as more than 11% BW, the antenna accomplishes the desired design goals for its use in 60 GHz applications. One trade-off on the fabrication of this device is that it combines separate methods for making each of the layers. The components are fabricated in different facilities. This adds more steps to the process and consequently makes it a more complex fabrication than the PCB version and other comparable antennas.

As a next step, the addition of reconfigurability and other smart-antenna techniques to the current antenna remain to be explored. A reconfigurable antenna is one that can be reconfigured in its structural geometry. With this, properties such as its main frequency, polarization, and/or radiation pattern can be changed [32]. This makes the antenna more useful for current high-throughput wireless communication technologies. Reconfigurable antennas add a degree of freedom to a communication system [33]. There are several methods that can be explored for creating the reconfigurable antenna. The research group has knowledge in the use of MEMS switches, PIN diodes, and parasitic layers [27]. Studying the addition of a parasitic layer and subsequently researching on other means of reconfigurability are the following steps.

5.1 The PCB Alternative

The PCB model was discarded and not fabricated because the smaller dimensions (distances as short as 10 µm) of the transmission lines could not be obtained by commonly available PCB fabrication processes. The designed PCB antenna shows comparable per-

formance parameters to the finished PCB + Quartz product, with room for improvement. The impedance bandwidth covers the entire 59-66 GHz band (see Figure 5.1).

A maximum realized gain over 18 dB is observed on the broadside direction (see Figure 5.2). Although fluctuating, the gain remains over 15.5 dB across the entire frequency band (Figure 5.3).

With a PCB fabrication technique which enables features as little as 10 µm in width, the designed PCB model can be fabricated. This antenna would have a shorter and cheaper fabrication process when compared to the Quartz + PCB antenna. If a wider probe is available, the transmission line dimensions can be modified and the array can be fabricated with a milling machine. For the sake of documentation, the critical design parameters of the PCB antenna array are given in Table 5.1. Figure 5.4 shows a simulated model of the PCB antenna.

On the early stages of the design process several types of transmission lines were tried before settling on using CPW. An aperture-coupled 2×1 array (on quartz) with a Wilkinson power divider is among these. As presented earlier, the CPW feed network needs the addition of air bridges or wire bonding. That is a complex part of the fabrication. It is of interest to keep developing low-cost high-performance antennas, especially if the fabrication process can be made simpler and faster. Hence the development of an array on quartz or PCB using aperture coupling is an immediate research interest.

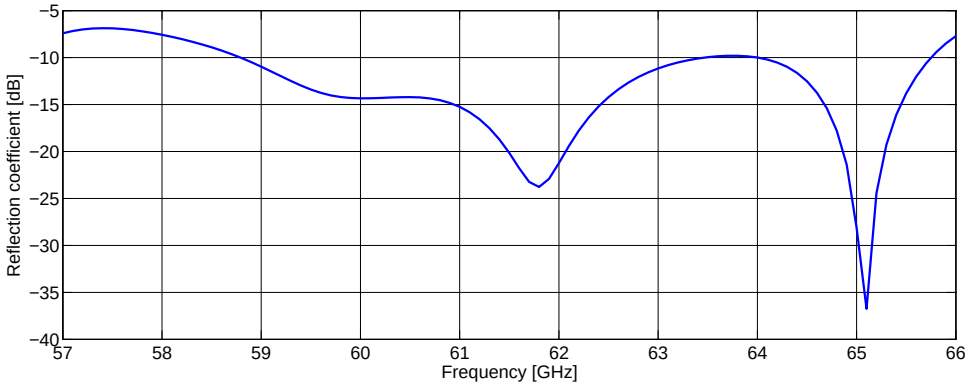

Fig. 5.1: Simulated reflection coefficient of the 16-element antenna array design on PCB

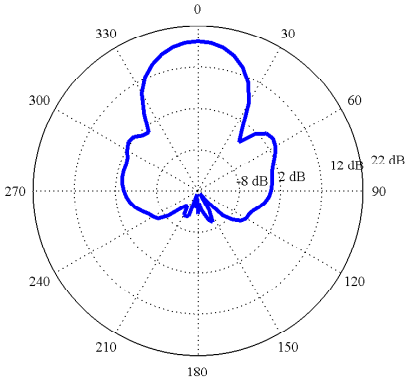

Fig. 5.2: Simulated radiation pattern of the 16-element PCB antenna on yz plane at 61 GHz

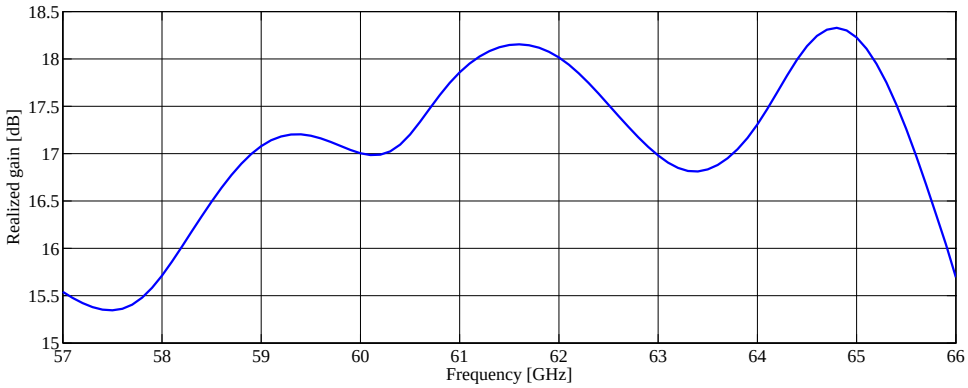

Fig. 5.3: Simulated realized gain across frequency on the broadside direction for the 16-element PCB antenna

Table 5.1: Design parameters of the 16-element PCB antenna array (dimensions in mm)

Parameter	Value	Parameter	Value
S	0.191	W	0.022827
L_l	1.15	L_w	1
L_t	0.04	P_l	1.1
P_w	1.8	L_Q	26
W_Q	33	Separation	$\frac{3}{4}\lambda_0$

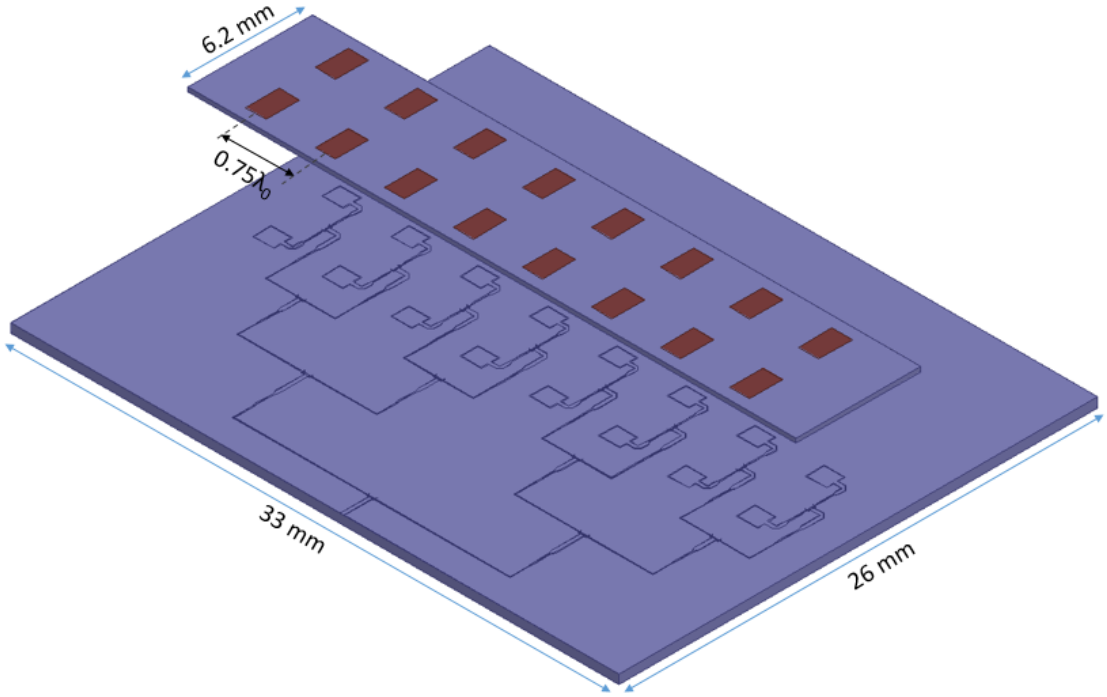

Fig. 5.4: 3-D view of the simulated 16-element PCB antenna array

References

[1] Cisco, "The zettabyte era: Trends and analysis (white paper)," 2015. [Online]. Available: http://www.cisco.com/c/en/us/solutions/collateral/service-provider/visual-networking-index-vni/VNI_Hyperconnectivity_WP.pdf

[2] Ericsson, "Ericsson mobility report: November 2015," 2015. [Online]. Available: http://www.ericsson.com/res/docs/2015/mobility-report/ericsson-mobility-report-nov-2015.pdf

[3] T. Lee, J. Jeong, J. Yoon, and J. Shin, "Adjustable subcarrier allocation for spectral efficiency and user fairness in 3gpp lte downlink systems," in *Advanced Communication Technology (ICACT), 2010 The 12th International Conference on*, vol. 2, Feb 2010, pp. 985–988.

[4] W. Roh, J. Y. Seol, J. Park, B. Lee, J. Lee, Y. Kim, J. Cho, K. Cheun, and F. Aryanfar, "Millimeter-wave beamforming as an enabling technology for 5G cellular communications: Theoretical feasibility and prototype results," *IEEE Communications Magazine*, vol. 52, no. 2, pp. 106–113, 2014.

[5] W.-f. Alliance, "Wigig and the future of seamless connectivity," pp. 3–5, 2013. [Online]. Available: http://www.wi-fi.org/file/wigig-and-the-future-of-seamless-connectivity-2013

[6] Wilocity, "Wilocity: Chipsets," 2013. [Online]. Available: http://wilocity.com/products/chipsets

[7] Peraso, "Peraso: Home Page," 2015. [Online]. Available: http://www.perasotech.com/

[8] Tensorcom, "Tensorcom extreme wireless: Products," 2015. [Online]. Available: http://www.tensorcom.com/products.html

[9] B. Leite, B. Martineau, A. Larie, A. Ghiotto, E. Kerhervé, and D. Belot, "60 GHz 28 nm CMOS transformer-coupled power amplifier for WiGig applications," *Electronics Letters*, vol. 50, no. 20, pp. 1451–1453, 2014. [Online]. Available: http://digital-library.theiet.org/content/journals/10.1049/el.2014.1979

[10] S. Jun and K. Chang, "A 60 GHz monopole antenna with slot defected ground structure for wigig applications," in *IEEE Antennas and Propagation Society, AP-S International Symposium (Digest)*, no. July. Orlando, FL: IEEE, 2013, pp. 2139–2140.

[11] M. Fakharzadeh and M. Mohajer, "An Integrated Wide-Band Circularly Polarized Antenna for Millimeter-Wave Applications," *IEEE Transactions on Antennas and Propagation*, vol. 62, no. 2, pp. 925–929, 2014.

[12] A. Tomkins, A. Poon, E. Juntunen, A. El-Gabaly, G. Temkine, Y.-L. To, A. Tabibiazar, M. Fakharzadeh, S. Jafarlou, H. Tawfik, B. Lynch, M. Tazlauanu, R. Glibbery, A. Overview, and C. Farnsworth, "Silicon Wireless Systems for 60-GHz Consumer and Infrastructure Applications," in *2014 IEEE Compound Semiconductor Integrated Circuit Symposium (CSICS)*. La Jolla, CA: IEEE, 2014, pp. 1–4. [Online]. Available: http://ieeexplore.ieee.org/xpls/abs{_}all.jsp?arnumber=6978578$\backslash$nhttp://ieeexplore.ieee.org/lpdocs/epic03/wrapper.htm?arnumber=6978578

[13] W. R. Read, K. W. Hillig II., E. A. Cohen, and H. M. Pickett, "The Measurement of Absolute Absorption of Millimeter Radiation in Gases: The Absorption of {CO} and {O_2}," *IEEE Transactions on Antennas and Propagation*, vol. 36, no. 8, pp. 1136–1143, 1988.

[14] A. Crawford and D. Hogg, "Measurement of atmospheric attenuation at millimeter wavelengths," *Bell System Technical Journal, The*, vol. 35, no. 4, pp. 907–916, July 1956.

[15] J. a. G. Akkermans and M. H. a. J. Herben, "Planar beam-forming array for broadband communication in the 60 GHz band," in *The Second European Conference on Antennas and Propagation*. Edinburgh: IET, 2007, pp. 1–6.

[16] D. Liu, J. a. G. Akkermans, H. C. Chen, and B. Floyd, "Packages with integrated 60-GHz aperture-coupled patch antennas," *IEEE Transactions on Antennas and Propagation*, vol. 59, no. 10, pp. 3607–3616, 2011.

[17] T. Seki, N. Honma, K. Nishikawa, and K. Tsunekawa, "A 60-GHz multilayer parasitic microstrip array antenna on LTCC substrate for system-on-package," *IEEE Microwave and Wireless Components Letters*, vol. 15, no. 5, pp. 339–341, 2005.

[18] R. Pilard, F. Gianesello, and D. Gloria, "60 GHz antennas and module development for WiGig applications: "Mm-wave antenna-systems" convened session," in *Proceedings of 6th European Conference on Antennas and Propagation, EuCAP 2012*. Prague: IEEE, 2012, pp. 2595–2598.

[19] W. Hong, K. H. Baek, and A. Goudelev, "Multilayer antenna package for IEEE 802.11ad employing ultralow-cost FR4," *IEEE Transactions on Antennas and Propagation*, vol. 60, no. 12, pp. 5932–5938, 2012.

[20] W. Liu, Z. N. Chen, and X. Qing, "60-GHz Thin Broadband High-Gain LTCC Metamaterial-Mushroom Antenna Array," *IEEE Transactions on Antennas and Propagation*, vol. 62, no. 9, pp. 4592–4601, 2014. [Online]. Available: http://ieeexplore.ieee.org/lpdocs/epic03/wrapper.htm?arnumber=6844007

[21] K. Wu, Y. J. Cheng, T. Djerafi, and W. Hong, "Substrate-integrated millimeter-wave and terahertz antenna technology," *Proceedings of the IEEE*, vol. 100, no. 7, pp. 2219–2232, 2012.

[22] H. Mopidevi, H. V. Hunerli, E. Cagatay, N. Biyikli, M. Imbert, J. Romeu, L. Jofre, and B. A. Cetiner, "Three-Dimensional Microfabricated Broadband Patch Antenna for WiGig Applications," *IEEE Antennas and Wireless Propagation Letters*, vol. 13, pp. 828–831, 2014. [Online]. Available: http://ieeexplore.ieee.org/lpdocs/epic03/wrapper.htm?arnumber=6803851

[23] ANSYS, "ANSYS HFSS," 2015. [Online]. Available: http://www.ansys.com/Products/Simulation+Technology/Electronics/Signal+Integrity/ANSYS+HFSS

[24] Keysight, "Advanced Design Systems (ADS)— Keysight (Agilent)," 2015. [Online]. Available: http://www.keysight.com/en/pc-1297113/advanced-design-system-ads?cc=US&lc=eng

[25] R. N. Simons, "Introduction," in *Coplanar Waveguide Circuits, Components, and Systems*. Wiley-IEEE Press, 2001, vol. 7, pp. 1–10. [Online]. Available: http://ieeexplore.ieee.org/xpl/articleDetails.jsp?arnumber=5237534

[26] N. Simons, "ConductorBacked Coplanar Waveguide," in *Coplanar Waveguide Circuits, Components, and Systems*. Wiley-IEEE Press, 2001, vol. 7, ch. 3, pp. 87–111. [Online]. Available: http://ieeexplore.ieee.org/xpl/articleDetails.jsp?arnumber=5237468

[27] H. Hunerli, H. Mopidevi, E. Cagatay, M. Imbert, J. Romeu, L. Jofre, B. Cetiner, and N. Biyikli, "Three dimensional microfabricated broadband patch and multifunction reconfigurable antennae for 60 GHz applications," in *2015 9th European Conference on Antennas and Propagation (EuCAP)*. Lisbon: IEEE, 2015, pp. 1–5. [Online]. Available: http://ieeexplore.ieee.org/xpls/abs{_}all.jsp?arnumber=7228902

[28] R. Garg, P. Bhartia, I. Rahl, and A. Ittipiboon, "Microstrip Antenna Design Handbook," in *Microstrip Antenna Design Handbook*. Artech House antennas and propagation library, 2001.

[29] K. Hettak, G. Delisle, G. Morin, and M. Stubbs, "A new type of array antennas fed by cpw for 60 ghz ism applications," in *Antennas and Propagation Society International Symposium, 2009. APSURSI '09. IEEE*, June 2009, pp. 1–4.

[30] R. N. Simons, "Coplanar Waveguide Discontinuities and Circuit Elements," in *Coplanar Waveguide Circuits, Components, and Systems*, 2001, vol. 7, ch. 9, pp. 237–287.

[31] B. University, "UNAM: Institute of Materials Science and Nanotechnology," 2015. [Online]. Available: http://unam.bilkent.edu.tr/

[32] B. Cetiner, L. Jofre, G. Li, and F. De Flaviis, "A packaged reconfigurable multielement antenna for wireless networking," in *Microwave Conference, 2001. APMC 2001. 2001 Asia-Pacific*, vol. 2, Dec 2001, pp. 705–708 vol.2.

[33] B. Cetiner, E. Akay, E. Sengul, and E. Ayanoglu, "A mimo system with multifunctional reconfigurable antennas," *Antennas and Wireless Propagation Letters, IEEE*, vol. 5, no. 1, pp. 463–466, Dec 2006.